THE JOURNAL OF PHYSICAL CHEMISTRY LETTERS
A JOURNAL OF THE AMERICAN CHEMICAL SOCIETY

pubs.acs.org/JPCL

Letter

Large-Area Three-Dimensional Displaced Overlapping Wing Perovskite Metamaterials with Giant Optical Chirality

Yuyi Feng, Xin Bi, Yifan Zeng, Yuxuan Dong, Hao Wang, Yanheng Wang, Qingyun Zhu, Clayton A. Nemitz, Jianyu Li, Zhongrui Wang, Tongtong Jiang, Fangci Zhang, Chenglei Jiang, Chunhui Zhang, Xianwen Liu, Guoguo Kang, Zhinong Yu, Ting Zhang, Yuwei Chai, Zefan Lin, Shuxian Du, Zhineng Lan, Peng Cui, Hao Huang, Yujie Qiu, Hengwei Qiu, Xing Zhao, and Meicheng Li*

Cite This: https://doi.org/10.1021/acs.jpclett.5c03955

Read Online

ACCESS | Metrics & More | Article Recommendations | Supporting Information

ABSTRACT: Perovskite chiral metamaterials have attracted widespread attention due to their enormous potential in areas such as chiral photoelectronics, spintronics, and ferroelectricity. However, current research often struggles to balance large-area fabrication with strong optical chirality responses. Here, we design and fabricate a novel three-dimensional displaced overlapping structure. A universal method combining electrochemical templating and stepwise glancing angle deposition enables large-area sample fabrication (1.4 cm × 1.4 cm). Ellipsometry-based circular dichroism measurements reveal a strong chiroptical response with a CD value of 12,149 mdeg and an anisotropy factor of 0.82 at 700 nm. Simulations indicate that the response originates from the resonant coupling of parallel electric and magnetic dipole components within the structure, with extrinsic chirality tunable via the incident light angle. Compared to conventional nanofabrication, this approach increases the production area by 4 orders of magnitude while offering tunable polarization conversion (1° to 32.6°). This work provides a viable pathway for developing large-area, low-cost polarizers, imaging, displays, and biosensors.

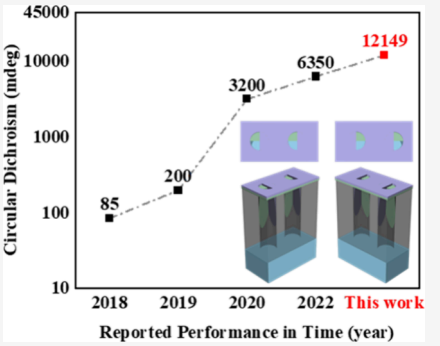

Chirality, the property of nonsuperimposability with one's mirror image, is widespread from macroscopic objects to microscopic molecules such as amino acids, sugars, and viruses. These chiral structures endow materials with distinct optical properties—including circular dichroism (CD) and circular birefringence (CB)—which provide effective means for detecting molecular chirality. However, such effects are usually weak in natural materials, limiting both nanoscale polarization control and the sensitivity of chiral spectroscopy. In contrast, artificially engineered chiral materials exhibit significantly stronger optical responses and have thus become a prominent research focus.[1−3]

Perovskites exhibit outstanding optoelectronic properties, making them promising for solar cells,[4] LEDs, and lasers.[5] Introducing chirality further extends their functionality into chiral photoelectronics[3] and spintronics,[6] enabling applications such as circularly polarized light detection,[7] emission,[8] spintronics,[9] biosensing[10] and nonlinear chiral optics.[11] Unlike metals, perovskites offer a tunable bandgap via halide composition, higher photoluminescence quantum yield, and lower optical loss, and perovskite-based devices provide unique capabilities beyond conventional plasmonic metals. Conventionally, chirality is imparted by embedding chiral molecules into the perovskite lattice. This approach allows for large-scale production and diverse material design. However, it typically results in weak circular dichroism and a low asymmetry factor (g), thereby limiting practical device performance. By combining perovskites with nanofabrication, meta-atoms can be designed with dimensions resonant at visible wavelengths, yielding stronger optical responses.

Conventional nanofabrication techniques—such as electron beam lithography, focused ion beam, and direct laser writing—enable the creation of precisely shaped chiral metamaterials with strong optical chirality.[12,13] However, these methods are generally costly and time-consuming, restricting large-scale production. Recent approaches have employed polystyrene sphere (PS) templates in glancing angle deposition or colloidal lithography to achieve larger-area chiral structures,[14] yet the isotropic nature of PS limits symmetry breaking and hence chiral response strength. In this work, we utilize anodic aluminum oxide (AAO) porous templates to fabricate chiral metamaterials with enhanced performance, which offers higher

Received: December 17, 2025
Revised: March 18, 2026
Accepted: March 24, 2026

Downloaded via UNIV COLLEGE LONDON on April 8, 2026 at 07:16:36 (UTC).
See https://pubs.acs.org/sharingguidelines for options on how to legitimately share published articles.

ACS Publications
© XXXX American Chemical Society

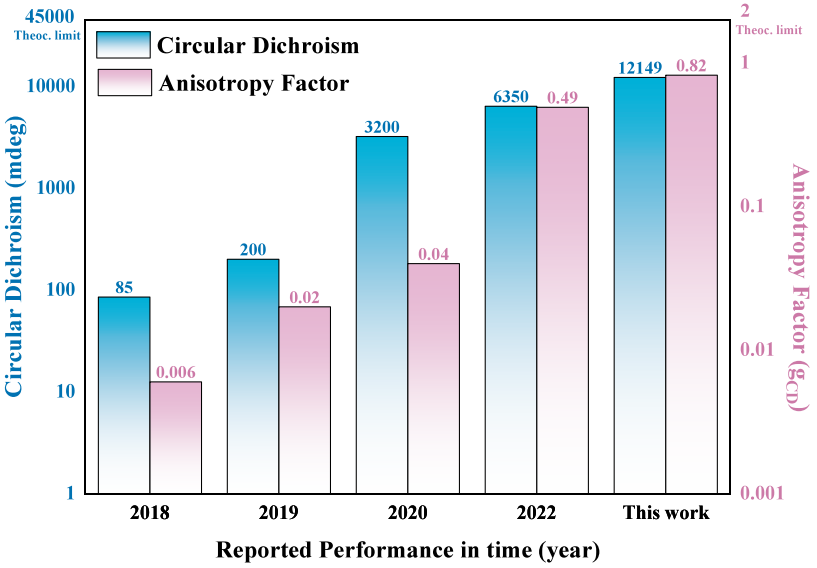

Figure 1. Comparison of our work with the performance of already reported results. In 2018, Sargent et al. demonstrated 85 mdeg CD and 0.006 g_{CD} in 2D bromide chiral perovskite films.[17] In 2019, Tang et al. achieved 200 mdeg CD and 0.02 g_{CD} in 1D chiral perovskite films for circularly polarized photodetection.[7] In 2020, Miyasaka et al. achieved a record CD of 3200 mdeg and g_{CD} of 0.04 in 1D chiral perovskite films through morphology optimization.[18] In 2022, Long et al. demonstrated a perovskite chiral metasurface achieving unprecedented CD (6350 mdeg) and g_{CD} (0.49) by shifting from structural to superstructural chirality via nanostructure engineering.[12] In this work, we fabricate large- area three-dimensional displaced overlapping wing perovskite metamaterials, achieving a CD of 12149 mdeg and a g_{CD} of 0.82.

mechanical and thermal stability,[15] as well as greater compatibility with vacuum deposition processes, making it advantageous for achieving pronounced chiral optical responses.[16]

In this work, we designed a three-dimensional displaced overlapping structure based on the classic helical chiral structure. Combining AAO templates and stepwise glancing angle deposition (GLAD), we successfully fabricated this structure by performing two tilted angle depositions on the aluminum oxide nanopore array template. The fabricated chiral structure exhibited remarkable chiral optical activity with a circular dichroism of up to 12,149 mdeg at a wavelength of 700 nm, as shown in Figure 1. The asymmetry factor reached 0.82. Furthermore, by varying the incident angle of light, we achieved tunable polarization conversion properties, with the maximum ellipticity at an incidence angle of 60°. With the aid of simulations, we thoroughly elucidate the mechanism behind the strong optical chirality response, which can be attributed to these different electromagnetic coupling modes. Moreover, a major advantage of this structure is its simple fabrication process. It does not rely on chiral templates or complex synthesis schemes, nor does it require multistep lithography processes, significantly simplifying the fabrication procedure and making it applicable to various materials. This work opens up new avenues for large-scale fabrication of perovskite chiral metamaterials with strong chiral optical activity.

The design concept is illustrated in Figure S3. Classic helical structures (I) possess a distinct left- or right-handed characteristic and exhibit drastically different optical responses to left- and right-circularly polarized light, resulting in strong circular dichroism (CD) responses. This phenomenon primarily arises from the parallel alignment of electric and magnetic dipoles leading to electromagnetic coupling. However, fabricating helical structures at the nanoscale is extremely challenging. Consequently, researchers have simplified them into stacked twisted nanorods (II). This was further simplified into a quasi-two-dimensional double nanorod structure (III). In this bimetallic nanorod structure, the chiral response primarily originates from a dipolar coupling mechanism: when two perpendicular gold nanorods are positioned close to a quarter of the wavelength apart, the electric dipole of one rod can effectively act as a magnetic dipole within the plane of the other rod.[19] This configuration enables the two nanorods to mimic an electric dipole and a magnetic dipole oriented in a parallel direction, leading to the generation of optical chirality.

The double-rod structure can form chiral structures and exhibit chiral optical responses through specific interlayer arrangement. However, the nanorods themselves still possess rotational symmetry. If the rectangular nanorods possessing C2-symmetry can be replaced with isosceles triangles which lack rotational symmetry(IV), the structural symmetry will be further broken, and the structure is expected to generate a stronger chiral optical response. Three-dimensional structures theoretically possess higher chiral optical responses due to the accumulative effect of light paths. Based on this design concept, we propose a three-dimensional "displaced overlapping wing" perovskite chiral metamaterial (V). Each individual wing structure breaks rotational symmetry, and the two wings overlap with a height difference, breaking the original mirror symmetry. Thus, the overall structure is assumed to achieve greater optical chirality.

A general fabrication method for three-dimensional "displaced overlapping wing" perovskite chiral metamaterials is presented. Step I: we fabricate the anodic aluminum oxide (AAO) nanopores on a transparent ITO glass, the details of which have been described in previous publications.[1] Step II: PbI_2 is vapor-deposited into the AAO nanopores to a thickness of 15 nm. Note that the substrate needs to be tilted relative to the lead iodide gas for unidirectional deposition. Step III: The sample, after one-time vapor deposition, is then divided into two parts. Step IV: The two halves of the sample are rotated 90° counterclockwise and then tilted 60° to the right (L-, step

https://doi.org/10.1021/acs.jpclett.5c03955
J. Phys. Chem. Lett. XXXX, XXX, XXX−XXX

IV left) and left (R-, step IV left), respectively. The vapor deposition step is repeated for both halves. This two-step tilted vapor deposition process produces a nanorod array with mirror geometric shapes. L- can be obtained by rotating the substrate counterclockwise, while R- can be obtained by rotating it clockwise. Step V: a MAI (methylammonium iodide) solution is spin-coated onto the PbI_2 surface, to allow $MAPbI_3$ (methylammonium lead triiodide) growth on the surface, and annealed to obtain the final perovskite chiral metamaterials, i.e. left-handed perovskite metamaterials (L-PVK) and right-handed perovskite metamaterials (R-PVK). More details regarding the preparation are provided in the Supporting Information.

To confirm the validity of our designed metamaterials, we conducted scanning electron microscopy (SEM) imaging on the cross-section of AAO pores where chiral perovskite metamaterials had been deposited (Figure 2b). The SEM

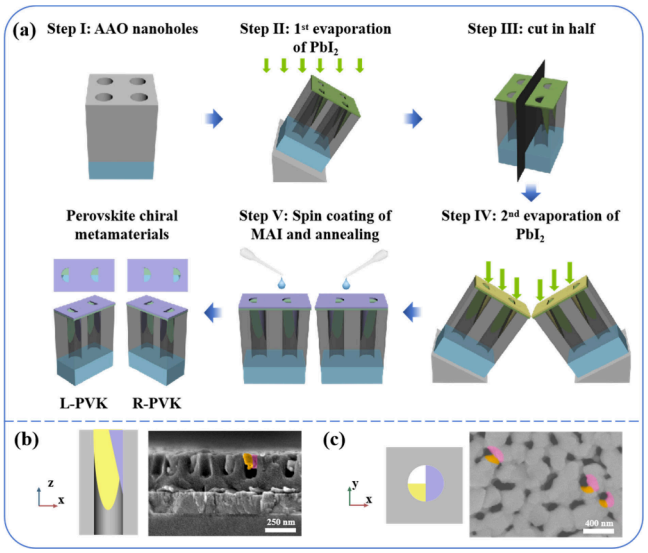

Figure 2. (a) Schematic illustration of the stepwise fabrication process for chiral perovskite metamaterials. Color coding: anodic aluminum oxide (AAO) template (gray); glass substrate (blue); first and second PbI_2 evaporation layers (green and yellow, respectively); $MAPbI_3$ conversion layer from the first PbI_2 deposition (green crescent); $MAPbI_3$ conversion layer from the second PbI_2 deposition (purple). (b) Cross-sectional SEM image of the fabricated structure. (c) Top-view SEM image of the fabricated structure with corresponding structural diagram. Color coding: perovskite from first deposition (yellow); perovskite from second deposition (purple); wing structures (pink and orange).

images show that both PbI_2 deposition layers adhere to one side of the pore wall and overlap asymmetrically, forming a wing-like displaced structure, consistent with our designed chiral structure. From a top-down perspective (Figure 2c), most of the deposited perovskite structures occupy about three-quarters of the entire nanopore, which also aligns with our design. The transmission electron microscopy (TEM) images in Figure S1 further validate our structure. Furthermore, cross-sectional EDS mapping in Figure S2 confirms the structural uniformity and integrity. Therefore, we can conclude that fabricating chiral metamaterials arrays using this stepwise tilted deposition method is feasible.

Figure S4 shows the reflection spectra of a set of chiral perovskite metamaterials fabricated experimentally, measured under p- and s-polarized light at different angles of incidence. Taking the left-handed enantiomer as an example (Figure S4a), at an incidence angle of 20°, the spectral curves for both p- and s-polarizations are relatively close, indicating that the current anisotropy is relatively weak. As the incidence angle increases, the reflection spectra of p- and s-polarized light show different trends. The reflection spectrum of p-polarization gradually flattens with increasing incidence angle, while the reflection spectrum of s-polarization becomes sharper, specifically with an increasing peak value at 580 nm. These results show that as the incidence angle increases, the difference between the reflection spectra excited by p- and s-polarized light gradually increases, indicating that the system exhibits enhanced anisotropy. We also observed that, under small incidence angles, the deviation between the p- and s-polarized spectra is mainly limited to the range 580−700 nm. As the incidence angle increases, the deviation between the spectra increases, showing strong anisotropy within a broader wavelength range of 400−900 nm at a large incidence angle (60°). To further understand this behavior, we plotted two-dimensional maps of reflection as a function of wavelength and incidence angle for both p- and s- excitations (Figure S4b,c). These plots show that under p-polarization, the reflectivity at 580 nm gradually decreases with increasing incidence angle, while under s-polarization it gradually increases, demonstrating an increase in anisotropy. Simultaneously, as the incidence angle increases, the range of anisotropy also gradually expands. For the right-handed enantiomer (Figure S4d−f), the trend of angle-dependent anisotropy change is similar to that of the left-handed enantiomer.

To obtain the authentic circular dichroism (CD) of perovskite metamaterials, we employed ellipsometry. Unlike apparent CD acquired through conventional measurements, which contains combined contributions from linear dichroism (LD), linear birefringence (LB), and authentic CD, this technique enables decoupling of LD and LB from the apparent CD, thereby obtaining the authentic CD.[20] To evaluate the chiral optical activity of perovskite chiral metamaterials, we measured the elliptic polarization parameters (Ψ, Ψps, Ψsp) and (Δ, Δps, Δsp), which represent the amplitude ratio and phase difference between linearly polarized components, respectively, for incidence angles ranging from 20° to 60° (J. A. Woollam VASE). We then obtained the complete reflection coefficient of the complex Jones matrix **R**, namely, R_{pp}, R_{ps}, R_{sp}, and R_{ss}. The detailed derivation process can be found in the previous work. The reflection matrix governing circularly polarized light is derived through a transformation of the basis vectors from linear to circular polarization states, as shown by the eq 1 below:

$$\begin{pmatrix} R_{rr} & R_{rl} \\ R_{lr} & R_{ll} \end{pmatrix} = \frac{1}{2}\begin{pmatrix} R_{pp} - R_{ss} + i(R_{ps} + R_{sp}) & R_{pp} + R_{ss} - i(R_{ps} - R_{sp}) \\ R_{pp} + R_{ss} + i(R_{ps} - R_{sp}) & R_{pp} - R_{ss} - i(R_{ps} + R_{sp}) \end{pmatrix} \quad (1)$$

where r and l represent right-handed (RCP) and left-handed (LCP) circular polarizations, respectively.

Here, the CD signal is defined as $CD = \frac{180000}{\pi} \arctan \frac{\sqrt{R_{RCP}} - \sqrt{R_{LCP}}}{\sqrt{R_{RCP}} + \sqrt{R_{LCP}}}$, and $g = 2(R_{RCP} - R_{LCP})/(R_{RCP} + R_{LCP})$, which represents the ratio of the difference in reflection

https://doi.org/10.1021/acs.jpclett.5c03955
J. Phys. Chem. Lett. XXXX, XXX, XXX−XXX

intensities between right- and left-circularly polarized light to their sum. With $R_{RCP} = |R_{rr}|^2 + |R_{lr}|^2$ and $R_{LCP} = |R_{ll}|^2 + |R_{rl}|^2$, we obtained the reflection spectra for circularly polarized excitation, as shown in Figure 3a–f. Herein, anisotropy factor of experimental samples are presented in Figure S5, and CD values are presented in Figure 4a,b.

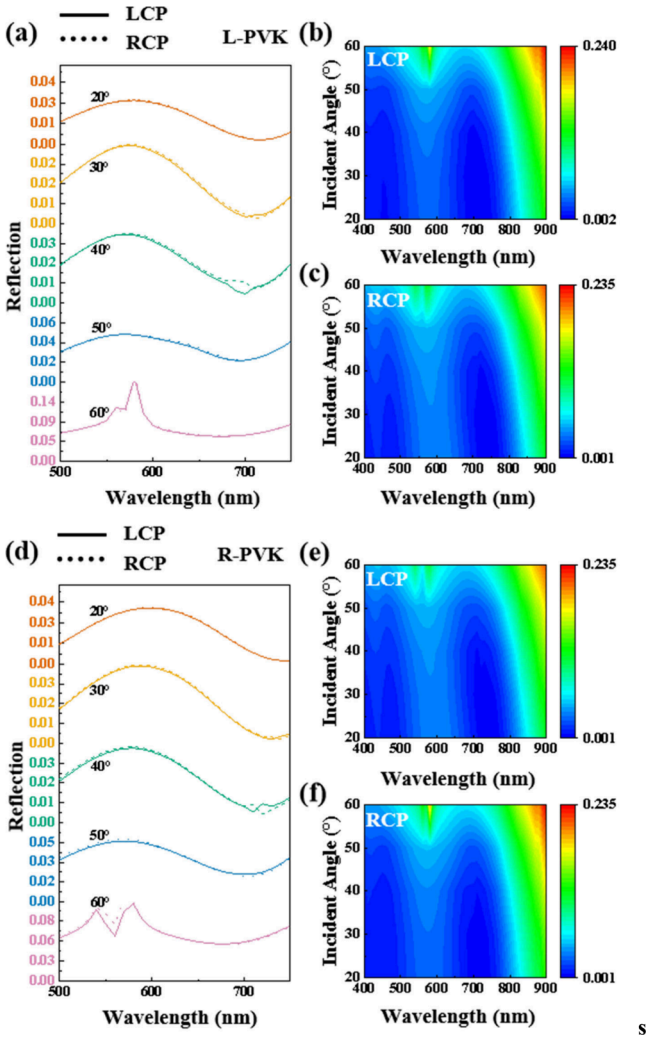

Figure 3. Experimental reflection under circularly polarized excitation. (a),(d) Reflection spectra of the sample at different angles of incidence of left and right circularly polarized (LCP and RCP) light. (b),(c) Contour mappings of reflection spectra for L-PVK under LCP light and RCP light, respectively. (e),(f) Contour mappings of reflection spectra for R-PVK under LCP light and RCP light, respectively.

Taking the left-handed enantiomer as an example, at incidence angles of 20° and 50°, the difference between LCP and RCP is relatively small across the entire measured wavelength range, resulting in a weak CD response (Figure 4a). At an incidence angle of 60°, a noticeable difference between RCP and LCP is observed near 560 nm, leading to a discernible CD signal (Figure 4a). At incidence angles of 30° and 40°, a significant difference between LCP and RCP emerges within a narrow band around 670–700 nm, resulting in strong CD signals. The maximum value reaches 12149 mdeg at 700 nm with an incident angle of 40° (Figure 4a).

We also show a comparison of the circular dichroism responses of the L-PVK and R-PVK enantiomers at an incidence angle of 40° in Figure 4c. Mirror-symmetric L-PVK and R-PVK enantiomers exhibit almost symmetrical CD characteristics. The strong CD response displayed by the chiral structure is caused by both its inherent chirality and the extrinsic chirality.[21] This is because: first, the chiral structure satisfies the asymmetric condition, possessing large structural chirality, which results in inherent optical chirality; second, the CD response of this structure is significantly affected by the incident angle, implying that it also possesses certain extrinsic chirality.

The plots also show that the circular dichroism exhibited by the enantiomers is not completely symmetric, and R-PVK shows a certain red shift phenomenon compared to L-PVK. When the incident light is tilted, the extrinsic chirality CD response is produced, simultaneously influencing the CD response exhibited by the inherent chirality. In other words, the CD response under tilted incidence is not a simple combination of inherent and extrinsic chirality.[22] It involves more complex interactions, ultimately leading to a circular dichroism response that is not completely symmetrical between the chiral enantiomers.

Furthermore, Figure 4d shows the cross-polarized and copolarized reflection amplitude spectra at an incident angle of 40°. Notably, the cross-polarized component exhibits a significant difference near 700 nm. Combining this with the CD spectrum results in Figure 4c, we find that the cross-polarized component primarily contributes to the strong CD response, more than the copolarized counterpart. This contrasts with previous literature on metal-based CD responses, where copolarized components were found to be dominant. This is perhaps because Mie scattering dominates the chiral optical response in perovskites, while plasmonic resonance dominates in metals. To demonstrate the primary influence of the chiral structure on the CD response, we prepared a control group with normally deposited perovskite within AAO nanopores, which is achiral at a subwavelength scale. Figure S6 shows the CD response of the control group, revealing a negligible and near-zero response. The weak signal observed is attributed to surface roughness and oblique-incidence reflection, whereas the GLAD-processed experimental group demonstrates significantly enhanced CD response (Figure 4). This confirms that the observed chiral response originates primarily from the inherent and extrinsic chirality of our designed metamaterials. Figures 4b,c,e,f display the two-dimensional distribution of CD for both enantiomers under LCP and RCP illumination. Previous research showed a linear curve pattern in metallic materials attributed to the surface plasmon polariton resonance mode,[23] while this study observes a sinusoidal curve pattern in perovskite materials, indicating a significant difference. This discrepancy is likely due to variations between Mie resonance modes in all-dielectric materials and plasmonic resonance modes in metals. The chiral resonance mode present in perovskites contributes to stronger optical chirality responses. Further research on quantitative resonance models for all-dielectric materials is needed.

To further investigate the physical mechanism underlying the strong chiral optical activity of the chiral PVK structure, we employed COMSOL to simulate its electric and magnetic field distributions at a horizontal cross-section. The refractive index of alumina used in the simulation is taken from the built-in material library of COMSOL, while the refractive index data of

https://doi.org/10.1021/acs.jpclett.5c03955
J. Phys. Chem. Lett. XXXX, XXX, XXX−XXX

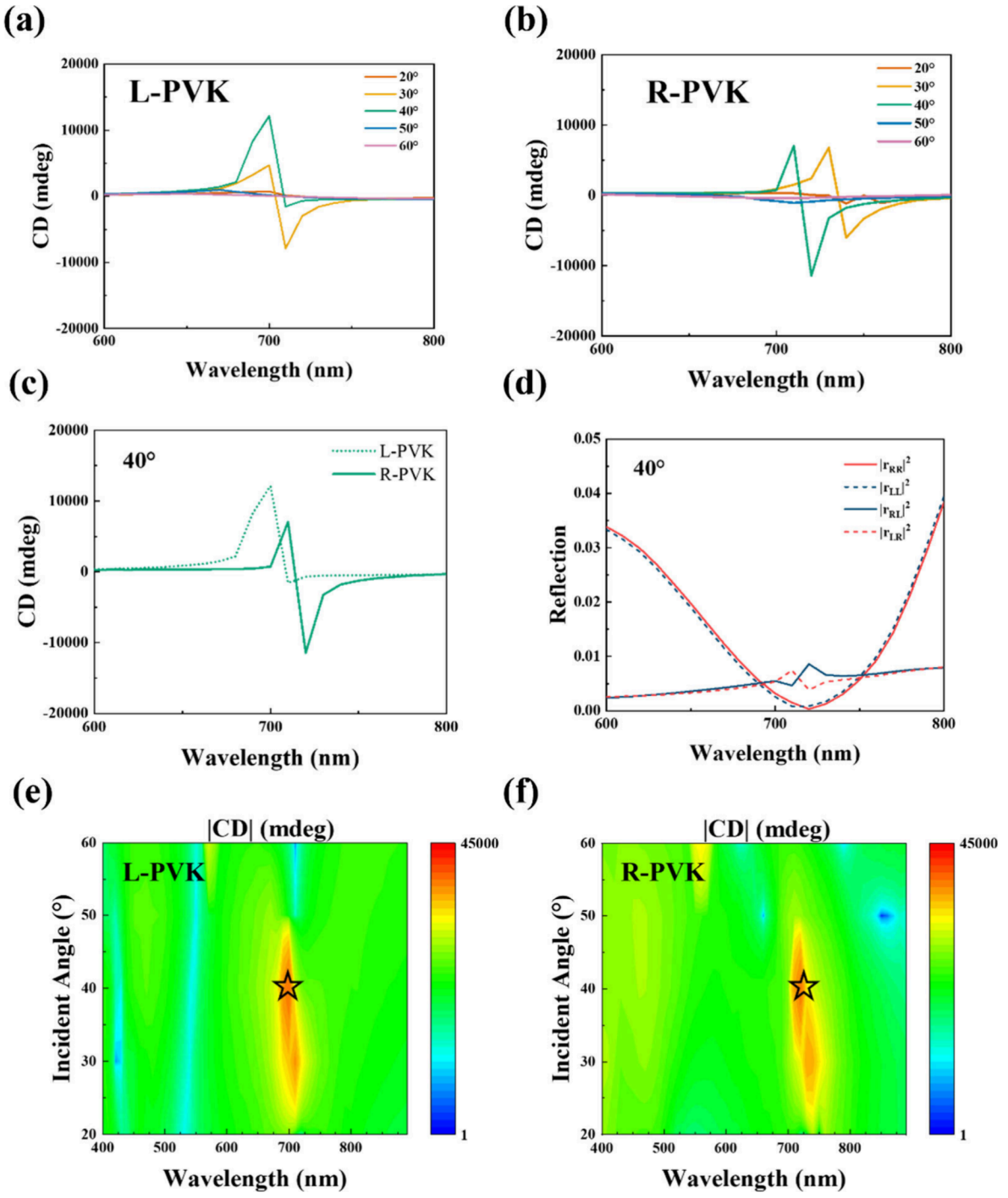

Figure 4. Circular dichroism response under circularly polarized excitation. (a,b) Reflection CD spectra of L-PVK and R-PVK at different angles of incidence, respectively. (c) Comparison of CD spectra of L-PVK and R-PVK at angle of incidence of 40°. (d) Copolarization and cross-polarization spectra corresponding to panel c. (e,f) Contour mappings of CD spectra.

$MAPbI_3$ comes from the measurements reported by Löper et al.[24] In the model, the optical path is incident along the $-Z$ direction, with Floquet periodic boundaries applied on the sides and perfectly matched layers (PML) implemented at the top and bottom. The simulated CD spectra are shown in Figure S7, while Figure 5a presents the simulated electric charge distribution and magnetic field vector distribution within the *xy* plane of the chiral structure. To investigate the chiral response, we analyzed the fields at 700 nm (Figure 5a) under 40° incidence. Under irradiation with RCP light at a wavelength of 700 nm, electric dipoles predominantly point toward the upper right. Combining this observation with the magnetic field vector distribution, we can deduce that the direction of the magnetic dipole aligns approximately parallel to the electric dipole. According to a generalization of the Rosenfeld criterion, which states that an optical activity response can only be observed when the dot product of the electric and magnetic dipoles (p·m) is nonzero, the parallel alignment of these dipoles in our structure leads to a strong chiral optical response. Similarly, under illumination with LCP

https://doi.org/10.1021/acs.jpclett.5c03955
J. Phys. Chem. Lett. XXXX, XXX, XXX−XXX

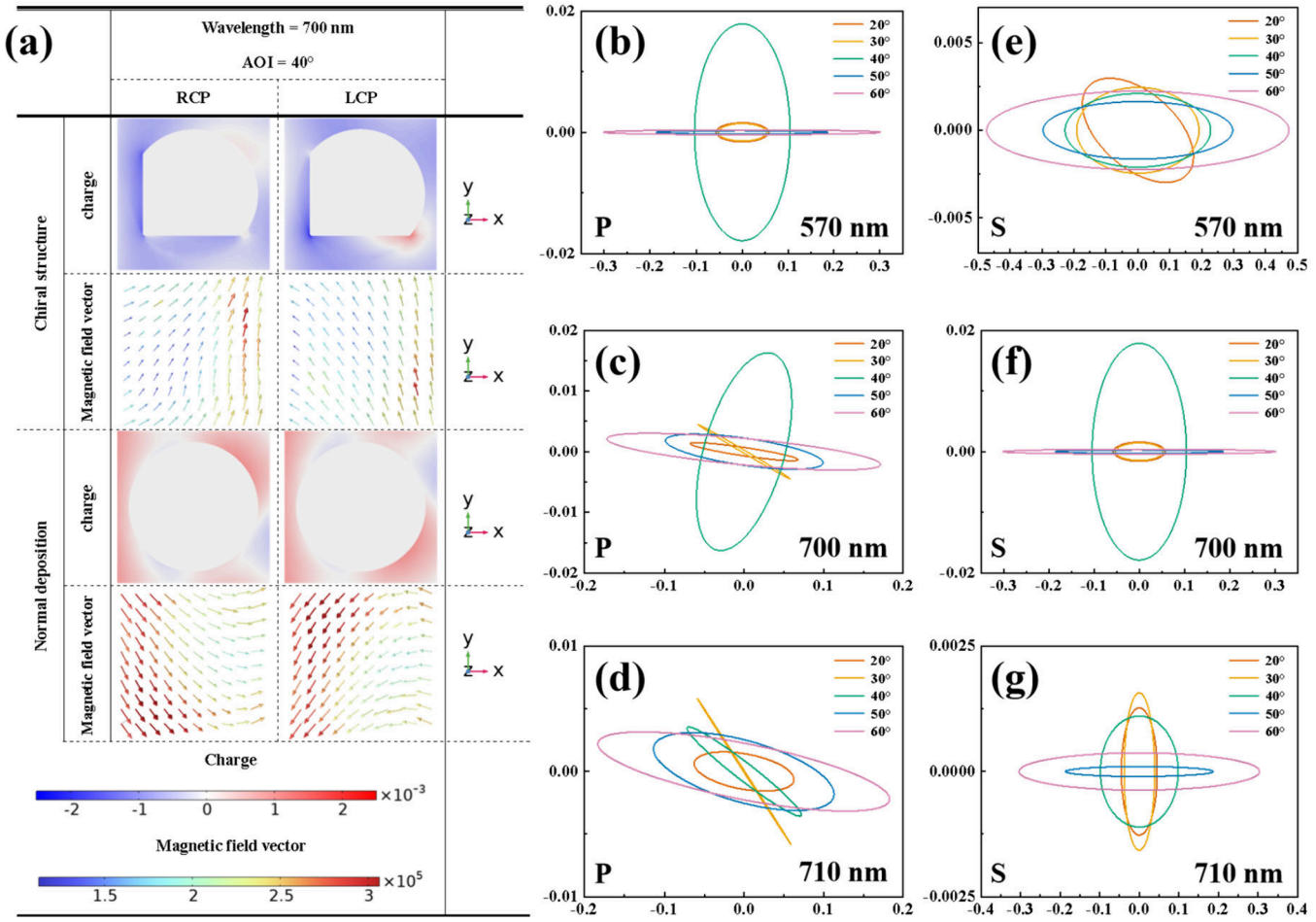

Figure 5. (a) The electric field and magnetic field distributions on the cross-section of the *XY* plane under the excitation of circular polarized light at 700 nm. (b–d) Polarization-state ellipses for the reflected light when the input wave is p-polarized light, at wavelengths of 570, 690 and 710 nm, respectively. (e–g) Polarization-state ellipses for the reflected light when the input wave is s-polarized light, corresponding to panels a–c.

light at 700 nm, the electric and magnetic dipoles exhibit a nonparallel orientation compared to RCP irradiation, resulting in a distinct difference in their interaction angle. Consequently, this results in different chiral optical responses for the two polarizations. This discrepancy contributes to the strong CD response observed in the chiral wing structure at 700 nm, primarily due to the contrasting interactions between electric and magnetic dipoles on the left wing under RCP and LCP illumination.

When linearly polarized light waves are incident on optically active and anisotropic media, their polarization state will be transformed from linear to elliptical. To investigate the application of chiral structures in polarization conversion, we exhibit its output polarization spectrum (Figure 5b–g) and the corresponding ellipticity angle. The output polarization ellipses shown in the figure illustrate the tunable polarization conversion achievable by varying the incidence angle and wavelength when the chiral metamaterial is illuminated with linearly polarized light. The ellipticity angle (η) is defined such that tan η equals the ratio of the short axis of the ellipse to its long axis. An ellipticity angle of +45° indicates right-circular polarization, while −45° corresponds to left-circular polarization. Under excitation with short-wavelength (570 nm) p-polarized light, as the incident angle changes, the ellipticity angle remains roughly 1°, approaching linear polarization. However, at an incident angle of 60°, the ellipticity angle reaches 32.9°, approaching circular polarization, demonstrating strong polarization conversion performance. Under s-polarized light excitation, the ellipticity angles for different incident angles are close to 1°, showing weak polarization conversion performance. When the wavelength increases to 690 nm, at a 40° incident angle, the ellipticity angles under p-polarized and s-polarized light are 8.7° and 5.3°, respectively, exhibiting strong polarization conversion performance. When the wavelength further increases to 710 nm, L-PVK also exhibits some polarization conversion performance at a 30° incident angle, with an ellipticity angle of 2.3°. The polarization conversion performance exhibited by the sample is mainly due to the combined effect of CD and CB (Figure S8) responses.[25] The chiral metamaterials show strong polarization conversion performance at specific angles and wavelengths, and exhibit tunable polarization conversion characteristics as a function of wavelength and incident angle.

This work demonstrates the fabrication of chiral perovskite metamaterials with strong optical activity. Combining electrochemical templates with stepwise GLAD method, we successfully fabricated three-dimensional displaced overlapping structures with strong optical chirality and anisotropy within nanopores through two-step tilted deposition combined with solution engineering strategies. Experimental and simulation results show that the strong optical chiral response stems from the intense coupling of electric and magnetic dipoles within the

https://doi.org/10.1021/acs.jpclett.5c03955
J. Phys. Chem. Lett. XXXX, XXX, XXX−XXX

wing-shaped structure, ultimately resulting in a high circular dichroism (up to 12149 mdeg) and a high asymmetry factor (up to 0.82). The distinct CD responses observed under different wavelengths are attributed to varying electromagnetic coupling modes between the wings, revealing a clear bisignate characteristic. The strong chiral optical response arises from both the inherent chirality of the metamaterials and the extrinsic chirality introduced by the incident wave vector interacting with the structure, further enhancing its overall chiral optical performance. Moreover, the output polarization ellipse can be finely tuned by changing the angle of the incident linearly polarized light. Due to its strong circular dichroism, tunable polarization response, and large-scale fabrication capabilities, this device holds promise for applications in chiral biosensing, polarizers, catalysis, and other fields. We propose that the of the fabrication strategy also provides a new avenue for the design of future chiral architectures, which can be further optimized by adjusting the nanopore dimensions, deposition thickness, vapor incidence angle, and other relevant parameters.

■ ASSOCIATED CONTENT

Supporting Information

The Supporting Information is available free of charge at https://pubs.acs.org/doi/10.1021/acs.jpclett.5c03955.

Experimental methods including fabrication of metamaterials and characterization; TEM image of metamaterials; cross-sectional characterization of the chiral perovskite metamaterial; schematic design principle for overlapping wing chiral metamaterials; experimental reflection under linearly polarized excitation; circular dichroism (CD) response and anisotropy factor (g) of experimental samples; circular dichroism response of control sample; parametric simulation of overlapping height effects on chiroptical response; COMSOL simulation structure schematic and simulated circular dichroism response of L-PVK and R-PVK; electric field and magnetic field distributions on the cross-section of XY plane under the excitation of circular polarized light at 580 and 600 nm; circular birefringence of (a) L-PVK and (b) R-PVK; XRD spectra of $CH_3NH_3PbI_3$ perovskite (PDF)

■ AUTHOR INFORMATION

Corresponding Author

Meicheng Li − *State Key Laboratory of Alternate Electrical Power System with Renewable Energy Sources, School of New Energy, North China Electric Power University, Beijing 102206, China;* orcid.org/0000-0002-0731-741X; Email: mcli@ncepu.edu.cn

Authors

Yuyi Feng − *State Key Laboratory of Alternate Electrical Power System with Renewable Energy Sources, School of New Energy, North China Electric Power University, Beijing 102206, China; Qinghai Province Institute for Product Quality Inspection & Testing, Qinghai 810017, China*

Xin Bi − *State Key Laboratory of Alternate Electrical Power System with Renewable Energy Sources, School of New Energy, North China Electric Power University, Beijing 102206, China*

Yifan Zeng − *State Key Laboratory of Alternate Electrical Power System with Renewable Energy Sources, School of New Energy, North China Electric Power University, Beijing 102206, China*

Yuxuan Dong − *State Key Laboratory of Alternate Electrical Power System with Renewable Energy Sources, School of New Energy, North China Electric Power University, Beijing 102206, China*

Hao Wang − *State Key Laboratory of Alternate Electrical Power System with Renewable Energy Sources, School of New Energy, North China Electric Power University, Beijing 102206, China*

Yanheng Wang − *State Key Laboratory of Alternate Electrical Power System with Renewable Energy Sources, School of New Energy, North China Electric Power University, Beijing 102206, China*

Qingyun Zhu − *Qinghai Province Institute for Product Quality Inspection & Testing, Qinghai 810017, China*

Clayton A. Nemitz − *Department of Physics and Astronomy, University of North Carolina, Chapel Hill, North Carolina 27516, United States*

Jianyu Li − *State Key Laboratory of Alternate Electrical Power System with Renewable Energy Sources, School of New Energy, North China Electric Power University, Beijing 102206, China*

Zhongrui Wang − *State Key Laboratory of Alternate Electrical Power System with Renewable Energy Sources, School of New Energy, North China Electric Power University, Beijing 102206, China*

Tongtong Jiang − *State Key Laboratory of Alternate Electrical Power System with Renewable Energy Sources, School of New Energy, North China Electric Power University, Beijing 102206, China*

Fangci Zhang − *State Key Laboratory of Alternate Electrical Power System with Renewable Energy Sources, School of New Energy, North China Electric Power University, Beijing 102206, China*

Chenglei Jiang − *State Key Laboratory of Alternate Electrical Power System with Renewable Energy Sources, School of New Energy, North China Electric Power University, Beijing 102206, China*

Chunhui Zhang − *State Key Laboratory of Alternate Electrical Power System with Renewable Energy Sources, School of New Energy, North China Electric Power University, Beijing 102206, China*

Xianwen Liu − *School of Optics and Photonics, Beijing Institute of Technology, Beijing 100081, China*

Guoguo Kang − *School of Optics and Photonics, Beijing Institute of Technology, Beijing 100081, China*

Zhinong Yu − *School of Optics and Photonics, Beijing Institute of Technology, Beijing 100081, China;* orcid.org/0000-0002-4937-3858

Ting Zhang − *Laboratory of Optoelectronic Information Technology and Devices, Ningbo Institute of Materials Technology and Engineering, Chinese Academy of Sciences, Ningbo, Zhejiang 315201, China;* orcid.org/0009-0005-2778-7610

Yuwei Chai − *School of Optics and Photonics, Beijing Institute of Technology, Beijing 100081, China*

Zefan Lin − *School of Optics and Photonics, Beijing Institute of Technology, Beijing 100081, China*

Shuxian Du − *State Key Laboratory of Alternate Electrical Power System with Renewable Energy Sources, School of New*

https://doi.org/10.1021/acs.jpclett.5c03955
J. Phys. Chem. Lett. XXXX, XXX, XXX−XXX

Energy, North China Electric Power University, Beijing 102206, China

Zhineng Lan − *State Key Laboratory of Alternate Electrical Power System with Renewable Energy Sources, School of New Energy, North China Electric Power University, Beijing 102206, China*

Peng Cui − *State Key Laboratory of Alternate Electrical Power System with Renewable Energy Sources, School of New Energy, North China Electric Power University, Beijing 102206, China*

Hao Huang − *State Key Laboratory of Alternate Electrical Power System with Renewable Energy Sources, School of New Energy, North China Electric Power University, Beijing 102206, China*

Yujie Qiu − *State Key Laboratory of Alternate Electrical Power System with Renewable Energy Sources, School of New Energy, North China Electric Power University, Beijing 102206, China*

Hengwei Qiu − *State Key Laboratory of Alternate Electrical Power System with Renewable Energy Sources, School of New Energy, North China Electric Power University, Beijing 102206, China;* orcid.org/0000-0002-2947-0626

Xing Zhao − *State Key Laboratory of Alternate Electrical Power System with Renewable Energy Sources, School of New Energy, North China Electric Power University, Beijing 102206, China;* orcid.org/0000-0002-3323-2014

Complete contact information is available at: https://pubs.acs.org/10.1021/acs.jpclett.5c03955

Notes

The authors declare no competing financial interest.

■ ACKNOWLEDGMENTS

This work is supported partially by National Natural Science Foundation of China (Grant nos. 62405088, 52232008, 52102245, 52402254 and 22409061), Beijing Natural Science Foundation (Z240024, 2222076, 2222077), the project of China Three Gorges Corporation named key technologies of intelligent joint regulation and operation with grid connected friendly in power station group of wind, solar photovoltaic and energy storage (WWKY-2021-0173), Huaneng Group Headquarters Science and Technology Project (HNKJ20-H88), the Fundamental Research Funds for the Central Universities (2023MS042, 2023MS047, 2024MS036, 2024MS039) and the NCEPU "Double First-Class" Program.

■ REFERENCES

(1) Feng, Y.; Leiderer, P.; Zhao, R.; Xiao, X.; Giannini, V.; Maier, S. A.; Nemitz, C. A.; Lin, Z.; Ding, N.; Kang, G. Giant polarization anisotropic optical response from anodic aluminum oxide templates embedded with plasmonic metamaterials. *Opt. Express* **2020**, *28* (20), 29513−29528.

(2) Liu, Z.; Du, H.; Li, J.; Lu, L.; Li, Z.-Y.; Fang, N. X. Nano-kirigami with giant optical chirality. *Science advances* **2018**, *4* (7), No. eaat4436. Kong, X. T.; Besteiro, L. V.; Wang, Z.; Govorov, A. O. Plasmonic chirality and circular dichroism in bioassembled and nonbiological systems: theoretical background and recent progress. *Adv. Mater.* **2020**, *32* (41), 1801790. Mun, J.; Kim, M.; Yang, Y.; Badloe, T.; Ni, J.; Chen, Y.; Qiu, C.-W.; Rho, J. Electromagnetic chirality: from fundamentals to nontraditional chiroptical phenomena. *Light: Science & Applications* **2020**, *9* (1), 139. Kuzyk, A.; Schreiber, R.; Fan, Z.; Pardatscher, G.; Roller, E.-M.; Högele, A.; Simmel, F. C.; Govorov, A. O.; Liedl, T. DNA-based self-assembly of chiral plasmonic nanostructures with tailored optical response. *Nature* **2012**, *483* (7389), 311−314. Li, J.; Lu, X.; Li, H.; Song, C.; Tan, Q.; He, Y.; Liu, J.; Luo, L.; Tang, T.; Liu, T.; et al. Racemic dielectric metasurfaces for arbitrary terahertz polarization rotation and wavefront manipulation. *Opto-Electronic Advances* **2024**, *7* (10), 240075. Li, J.; Chen, L.; Xu, H.; Nan, T.; Lu, X.; Li, H.; Xu, W.; Tan, Q.; Li, J.; Lv, Y.; et al. Spin-dependent terahertz wavefront shaping based on hybrid phase in all-silicon chiral metasurfaces. *Photon. Res.* **2025**, *13* (5), 1271−1281. Zhe, Z.; Zhanyi, L.; Jialuo, D.; Jiaqi, Y.; Li, L.; Tingting, T.; Jie, L.; Jianquan, Y. Efficient angular dispersions manipulation of terahertz metasurface based on extrinsic chirality. *Opto-Electronic Engineering* **2025**, *52* (8), 250093.

(3) Long, G.; Sabatini, R.; Saidaminov, M. I.; Lakhwani, G.; Rasmita, A.; Liu, X.; Sargent, E. H.; Gao, W. Chiral-perovskite optoelectronics. *Nature Reviews Materials* **2020**, *5* (6), 423−439.

(4) Yan, H.; Zhao, X.; Huang, H.; Wu, D.; Zhu, P.; Li, D.; Fan, B.; Qiu, Y.; Yang, Y.; Geng, Q. Flocculating-regulated TiO2 deposition enables the synergistic effect of doping for perovskite solar cells with efficiency exceeding 25.8%. *Adv. Energy Mater.* **2025**, *15* (8), 2403200. Zhang, Q.; Huang, H.; Yang, Y.; Wang, M.; Qu, S.; Lan, Z.; Jiang, T.; Wang, Z.; Du, S.; Lu, Y. A universal ternary solvent system of surface passivator enables perovskite solar cells with efficiency exceeding 26%. *Adv. Mater.* **2024**, *36* (50), 2410390. Lan, Z.; Huang, H.; Lu, Y.; Qu, S.; Wang, M.; Du, S.; Yang, Y.; Sun, C.; Zhang, Q.; Suo, Y. Homogenizing the Electron Extraction via Eliminating Low-Conductive Contacts Enables Efficient Perovskite Solar Cells with Reduced Up-Scaling Losses. *Adv. Funct. Mater.* **2024**, *34* (32), 2316591.

(5) Chen, J.; Du, W.; Shi, J.; Li, M.; Wang, Y.; Zhang, Q.; Liu, X. Perovskite quantum dot lasers. *InfoMat* **2020**, *2* (1), 170−183.

(6) Privitera, A.; Righetto, M.; Cacialli, F.; Riede, M. K. Perspectives of Organic and Perovskite-Based Spintronics. *Advanced Optical Materials* **2021**, *9* (14), 2100215.

(7) Chen, C.; Gao, L.; Gao, W.; Ge, C.; Du, X.; Li, Z.; Yang, Y.; Niu, G.; Tang, J. Circularly polarized light detection using chiral hybrid perovskite. *Nat. Commun.* **2019**, *10* (1), 1927.

(8) Shi, Y.; Duan, P.; Huo, S.; Li, Y.; Liu, M. Endowing perovskite nanocrystals with circularly polarized luminescence. *Adv. Mater.* **2018**, *30* (12), 1705011. Nan, T.; Zhao, H.; Guo, J.; Wang, X.; Tian, H.; Zhang, Y. Generation of structured light beams with polarization variation along arbitrary spatial trajectories using tri-layer meta-surfaces. *Opto-Electronic Science* **2024**, *3* (5), 230052.

(9) Bloom, B. P.; Paltiel, Y.; Naaman, R.; Waldeck, D. H. Chiral Induced Spin Selectivity. *Chem. Rev.* **2024**, *124* (4), 1950−1991.

(10) Min, J.; Demchyshyn, S.; Sempionatto, J. R.; Song, Y.; Hailegnaw, B.; Xu, C.; Yang, Y.; Solomon, S.; Putz, C.; Lehner, L. E. An autonomous wearable biosensor powered by a perovskite solar cell. *Nature electronics* **2023**, *6* (8), 630−641.

(11) Liu, Y.; Gong, Y. P.; Geng, S.; Feng, M. L.; Manidaki, D.; Deng, Z.; Stoumpos, C. C.; Canepa, P.; Xiao, Z.; Zhang, W. X. Hybrid germanium bromide perovskites with tunable second harmonic generation. *Angew. Chem., Int. Ed.* **2022**, *61* (43), No. e202208875. Zheng, Y.; Xu, J.; Bu, X. H. 1D Chiral Lead Halide Perovskites with Superior Second-Order Optical Nonlinearity. *Advanced Optical Materials* **2022**, *10* (1), 2101545.

(12) Long, G.; Adamo, G.; Tian, J.; Klein, M.; Krishnamoorthy, H. N. S.; Feltri, E.; Wang, H.; Soci, C. Perovskite metasurfaces with large superstructural chirality. *Nat. Commun.* **2022**, *13* (1), 1551.

(13) Kilic, U.; Hilfiker, M.; Wimer, S.; Ruder, A.; Schubert, E.; Schubert, M.; Argyropoulos, C. Controlling the broadband enhanced light chirality with L-shaped dielectric metamaterials. *Nat. Commun.* **2024**, *15* (1), 3757. Zhang, L.; Wang, T.; Shen, Z.; Liu, M. Chiral nanoarchitectonics: towards the design, self-assembly, and function of nanoscale chiral twists and helices. *Adv. Mater.* **2016**, *28* (6), 1044−1059. Tang, H.; Rosenmann, D.; Czaplewski, D. A.; Yang, X.; Gao, J. Dual-band selective circular dichroism in mid-infrared chiral metasurfaces. *Opt. Express* **2022**, *30* (11), 20063−20075. Mamonov, E.; Kolmychek, I.; Murzina, T.; Maydykovsky, A.; Aktsipetrov, O.; Valev, V.; Verbiest, T.; Silhanek, A.; Moshchalkov, V. Circular

dichroism in optical second harmonic generated in reflection from chiral G-shaped metamaterials. *Journal of Physics: Conference Series* **2012**, *352*, 012029.
(14) Wang, Y.; Ai, B.; Wang, Z.; Guan, Y.; Chen, X.; Zhang, G. Chiral nanohelmet array films with Three-Dimensional (3D) resonance cavities. *J. Colloid Interface Sci.* **2022**, *626*, 334−344. Hou, Y.; Leung, H. M.; Chan, C. T.; Du, J.; Chan, H. L. W.; Lei, D. Y. Ultrabroadband optical superchirality in a 3D stacked-patch plasmonic metamaterial designed by two-step glancing angle deposition. *Adv. Funct. Mater.* **2016**, *26* (43), 7807−7816. Portal, S.; Corbella, C.; Arteaga, O.; Martin, A.; Mandal, T.; Kahr, B. Characterization of Chiral Nanostructured Surfaces Made via Colloidal Lithography. *Nanomaterials* **2023**, *13* (15), 2235. Yang, X.; Liu, Y.; Chen, F.-L.; Lin, Q.-Q.; Chikkaraddy, R.; Huang, S.-S.; Xian, S.-L.; Hou, Y.-D.; Du, J.-L.; Xia, L.-P. Stepwise colloidal lithography toward scalable and various planar chiral metamaterials. *Rare Metals* **2024**, *43* (2), 723−735.
(15) Yang, X.; Liu, Y.; Chen, F.-L.; Lin, Q.-Q.; Chikkaraddy, R.; Huang, S.-S.; Xian, S.-L.; Hou, Y.-D.; Du, J.-L.; Xia, L.-P.; et al. Stepwise colloidal lithography toward scalable and various planar chiral metamaterials. *Rare Metals* **2024**, *43* (2), 723−735.
(16) Feng, Y.; Kim, K.-D.; Nemitz, C. A.; Kim, P.; Pfadler, T.; Gerigk, M.; Polarz, S.; Dorman, J. A.; Weickert, J.; Schmidt-Mende, L. Uniform large-area free-standing silver nanowire arrays on transparent conducting substrates. *J. Electrochem. Soc.* **2016**, *163* (8), D447.
(17) Long, G.; Jiang, C.; Sabatini, R.; Yang, Z.; Wei, M.; Quan, L. N.; Liang, Q.; Rasmita, A.; Askerka, M.; Walters, G.; et al. Spin control in reduced-dimensional chiral perovskites. *Nat. Photonics* **2018**, *12* (9), 528−533.
(18) Ishii, A.; Miyasaka, T. Direct detection of circular polarized light in helical 1D perovskite-based photodiode. *Science advances* **2020**, *6* (46), No. eabd3274.
(19) Qiu, M.; Zhang, L.; Tang, Z.; Jin, W.; Qiu, C. W.; Lei, D. Y. 3D metaphotonic nanostructures with intrinsic chirality. *Adv. Funct. Mater.* **2018**, *28* (45), 1803147.
(20) Nicolas, M.; Walmsness, P. M.; Amboli, J.; Zhang, L.; Demesy, G.; Bonod, N.; Boujday, S.; Kildemo, M.; Gallas, B. True circular dichroism in optically active achiral metasurfaces and its relation to chiral near-fields. *ACS Applied Optical Materials* **2023**, *1* (8), 1360−1366. Zhang, Z.; Wang, Z.; Sung, H. H.-Y.; Williams, I. D.; Yu, Z.-G.; Lu, H. Revealing the intrinsic chiroptical activity in chiral metal-halide semiconductors. *J. Am. Chem. Soc.* **2022**, *144* (48), 22242−22250.
(21) Ren, M.; Plum, E.; Xu, J.; Zheludev, N. I. Giant nonlinear optical activity in a plasmonic metamaterial. *Nat. Commun.* **2012**, *3* (1), 833.
(22) Zhu, G.; Sun, Z.; Zhu, T.; Peng, W.; Fang, Y. Distinguishing Intrinsic and Extrinsic Chirality via Dynamic Polarizability Tensor Retrieval for Maximum Optical Activity. *ACS Applied Optical Materials* **2024**, *2* (6), 1209−1216.
(23) Hou, Y.; Qiu, M.; Cao, Z.; Zhou, J.; Ong, H. C.; Jin, W.; Du, J.; Lei, D. High-Q circular dichroism resonances in plasmonic lattices with chiral unit cells. *Adv. Funct. Mater.* **2022**, *32* (40), 2204095.
(24) Löper, P.; Stuckelberger, M.; Niesen, B.; Werner, J.; Filipič, M.; Moon, S.-J.; Yum, J.-H.; Topič, M.; De Wolf, S.; Ballif, C. Complex Refractive Index Spectra of CH3NH3PbI3 Perovskite Thin Films Determined by Spectroscopic Ellipsometry and Spectrophotometry. *J. Phys. Chem. Lett.* **2015**, *6* (1), 66−71.
(25) Shi, Z.; Zhu, A. Y.; Li, Z.; Huang, Y.-W.; Chen, W. T.; Qiu, C.-W.; Capasso, F. Continuous angle-tunable birefringence with freeform metasurfaces for arbitrary polarization conversion. *Science advances* **2020**, *6* (23), No. eaba3367.

https://doi.org/10.1021/acs.jpclett.5c03955
J. Phys. Chem. Lett. XXXX, XXX, XXX−XXX